The Journal of Chemical Physics

RESEARCH ARTICLE | JANUARY 08 2025

Dielectric profile at the Pt(111)/water interface

Special Collection: 2024 JCP Emerging Investigators Special Collection

Jia-Xin Zhu ; Jun Cheng ; Katharina Doblhoff-Dier

J. Chem. Phys. 162, 024702 (2025)
https://doi.org/10.1063/5.0239284

AIP Publishing

The Journal of Chemical Physics ARTICLE pubs.aip.org/aip/jcp

Dielectric profile at the Pt(111)/water interface

Cite as: J. Chem. Phys. 162, 024702 (2025); doi: 10.1063/5.0239284
Submitted: 18 September 2024 • Accepted: 31 October 2024 •
Published Online: 8 January 2025

View Online Export Citation CrossMark

Jia-Xin Zhu,[1,a] Jun Cheng,[1,2,3,b] and Katharina Doblhoff-Dier[4,c]

AFFILIATIONS

[1] State Key Laboratory of Physical Chemistry of Solid Surfaces, iChEM, College of Chemistry and Chemical Engineering, Xiamen University, Xiamen 361005, China
[2] Laboratory of AI for Electrochemistry (AI4EC), IKKEM, Xiamen 361005, China
[3] Institute of Artificial Intelligence, Xiamen University, Xiamen 361005, China
[4] Leiden Institute of Chemistry, Leiden University, Leiden 2300 RA, The Netherlands

Note: This paper is part of the 2024 JCP Emerging Investigators Special Collection.
[a] **Electronic mail:** jiaxinzhu@stu.xmu.edu.cn
[b] **Electronic mail:** chengjun@xmu.edu.cn
[c] **Author to whom correspondence should be addressed:** k.doblhoff-dier@lic.leidenuniv.nl

ABSTRACT

The dielectric constant, although a simplified concept when considering atomic scales, enters many mean-field, electrochemical interface models and constant potential models as an important parameter. Here, we use *ab initio* and machine-learned molecular dynamics to scrutinize the behavior of the electronic contribution to $\varepsilon_r(z)$ as a function of distance z from a Pt(111) surface. We show that the resulting dielectric profile can largely be explained as a sum of the metallic response and the density-scaled water response at the interface. A slight enhancement of the dielectric response close to the surface can be explained by elongated, strongly polarizable orbitals induced by metal/water bonding. In spite of this enhancement, our results suggest the presence of a region with a very low dielectric constant close to the surface (where the orientational dielectric response does not kick in yet), even for water in contact with hydrophilic metallic interfaces. This region will restrict the double layer capacitance to relatively low values even at potentials where dielectric saturation does not play a role yet. This finding has implications on possible interpretations of double layer capacitances, the dependence of surface electric fields on the ion size, and on electrochemical kinetics.

I. INTRODUCTION

The electric double layer (EDL) is one of the most fundamental building blocks in electrochemistry.[1,2] The structure that solvent molecules and ions form at the EDL and the resulting potential profile at the interface have considerable influence on the energetics and kinetics of electrochemical reactions. The structure of the EDL and the interfacial potential profile have, hence, attracted great interest since the early stage of electrochemistry.

Often, it is mainly the structure of ions that is of interest. For example, the effect of ion type and concentration on electrochemical reactions is vividly discussed in the literature, in particular with respect to CO_2 reduction,[3–6] but also for hydrogen evolution.[5–10] In other cases, the potential profile will be more relevant than the exact structure of the interface. This is the case, for example, when determining Frumkin corrections to reaction rates.[11,12] A correct representation of the potential profile can also be expected to play a crucial role in constant potential methods, as developed in recent years to allow for *ab initio* calculations under applied bias in computational electrochemistry.[13–16]

Constant potential methods often make use of mean-field models of the electrolyte. These models are, however, highly sensitive to their parameterization.[17,18] One of the most important factors determining the potential profile at the interface (and thus also the interfacial capacitance) is the dielectric constant, which describes the response of the solvent to the electric field at the interface.[19–22]

Determining the dielectric constant at the interface is challenging (in fact, it is even questionable whether the dielectric constant, which is a mean-field concept, is still a valid concept at the atomic scale in heterogeneous systems such as the solid/liquid interface[23]). Educated guesses and approximations are, therefore, inevitable,

leading to interfacial mean-field models in which the dielectric constant differs drastically (see, e.g., Table 2 of Ref. 18).

In one of the most simplified descriptions, the dielectric constant ε_r is assumed to be constant and around six in the compact layer[24–27] and takes the value of bulk water (i.e., ~78[28]) for the remaining regions. A dielectric constant around six in the compact layer can be justified as follows:

- When assuming a compact layer with a width of $d \approx 3$ Å and $\varepsilon_r = 6$, one obtains a capacitance of $C = \varepsilon_0 \varepsilon_r / d \approx 20$ μF/cm^2—a value consistent with experimental results for many metal/electrolyte interfaces under conditions of high electrolyte concentrations and far from the potential of zero charge (pzc).[2,29]
- $\varepsilon_r = 6$ corresponds to the dielectric response of water once the rotational degrees of freedom are frozen.[30] Considering that molecule–surface interactions and dielectric saturation effects (i.e., all water molecules being preferentially aligned to the surface electric field already) likely play a role at the interface between a charged electrode and an aqueous electrolyte, a value of $\varepsilon_r = 6$ thus seems realistic.

Considering the strongly layered structure of the interface, a dielectric constant that is constant in the entire compact layer is, however, likely an oversimplification.

A better knowledge of the dielectric profile, i.e., how ε_r varies in space close to the interface, is needed, in particular as the profile of ε_r can influence the predictions and interpretations derived from mean-field models and experimental observations.

Currently, most studies targeting the dielectric profile at the interface are based on force field molecular dynamics,[31–34] which suffer not only from errors stemming from force field parameterization[35] (in particular at the interface, where good force fields have not been developed) but also from an approximate description of electron polarization at the interface.[36] To overcome these issues, *ab initio* molecular dynamics (AIMD) simulations have recently been utilized to compute the dielectric profile.[37] Despite the elegant implementation of a thermopotentiostat, this density functional theory (DFT)-based study suffers from two issues: First, the dielectric constant was extracted using a finite difference method. However, the cathode and anode show distinct dielectric profiles in these calculations, indicating conditions deviating from the pzc, without the exact potential being known. Second, the simulations were performed on Ne-like electrodes, which is little representative of realistic electrochemical interfaces.

In this work, we address the dielectric profile at the Pt(111)/water interface at the pzc. To do so, we make use of machine-learned potentials (MLPs) and extend the MD simulation timescale to a few nanoseconds. The dielectric response at the interface is further split into an electronic contribution and an orientational contribution. While the former is calculated by applying an electric field on the DFT level, the latter is approximated from the polarization fluctuation based on empirical atomic charges. Importantly, we find that even on a hydrophilic metallic surface such as Pt, the electronic dielectric response is low in the region outside the image charge plane, but below the first water region, suggesting the presence of a (narrow) "gap" region with a low dielectric constant as often suggested for graphite[38] and in agreement with Ref. 39. Furthermore, we explain the electronic polarizability at the surface by combining a density scaled electronic polarizability of water with the electronic polarizability of the metal and accounting for a change in the polarizability of surface-near water due to a change in the shape (and polarizability) of molecular orbitals.

II. METHODS

A. Molecular dynamics simulations

The Pt(111)/H_2O interface was modeled using a 3D periodic supercell containing two Pt(111)/water interfaces as shown in Fig. 1(a). A six atomic layer thick Pt(111) slab was used, with a surface unit cell of $p(6 \times 6)$ atoms. The Pt slabs were separated by 30 Å of water with 230 water molecules, leading to a water density of 1 ± 0.05 g/cm^3 far away from the Pt surfaces (i.e., at $z \geq 9$ Å, where z is the distance from the uppermost Pt layers) after equilibration.

Using a machine-learned potential (MLP; obtained as described in Sec. II B), molecular dynamics (MD) simulations were performed in the CP2K software package.[40] The canonical (NVT) ensemble was approximated via the Nosé–Hoover thermostat with a chain length of 3. The temperature was set to 330 K, and the time step used in the propagation was set to 0.5 fs. During the MD simulations, the

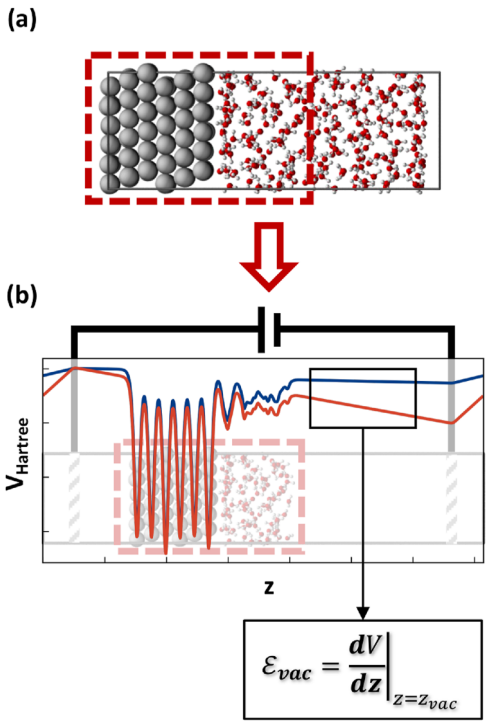

FIG. 1. Illustration of atomic models used. (a) 3D periodic supercell used in molecular dynamics simulations with machine-learned potentials and when computing the orientational dielectric constant. The red frame highlights atoms extracted when computing the electronic dielectric constant. (b) Setup used when computing the electronic dielectric constant. Dirichlet boundary conditions (DBCs) are applied in the z-direction as indicated by the charged plates and the external circuit. Red and blue lines: Hartree potential profiles V for two different DBCs. The slopes dV/dz in vacuum (highlighted by a black frame) provide ε_{vac}.

innermost two Pt layers are restrained by weak harmonic springs with a spring constant of 0.1 a.u. to ensure bulk properties.

B. Training and validation of the machine-learned potential

The MLP used in this work was trained with the DeePMD-kit software package.[41] Training data for the MLP were obtained from density functional theory (DFT) calculations performed in the CP2K software package.[40] The computational setup used in the DFT calculations is similar to that used in Ref. 42. In particular, PBE-D3 was used as exchange–correlation functional,[43,44] the ionic cores were described by Goedecker–Teter–Hutter (GTH) pseudopotentials with 1, 6, and 11 valence electrons for H, O, and Pt, respectively, and a double-ζ basis set with one set of polarization functions was employed. The plane wave energy cutoff was set to a high value of 1000 Ry to reduce the noise in the data and improve the fitting accuracy in the MLP training. All DFT calculations were based on calculations at the gamma point only.

A concurrent learning workflow DP-GEN was used to efficiently collect a training dataset that is fully representative for the configuration space. Each iteration of the concurrent learning workflow consists of a series of (i) training, (ii) exploration, and (iii) labeling.[45]

In the training step, a committee of four MLPs was trained based on the energies and forces. The Deep Potential Smooth Edition (DeepPot-SE) descriptor[46] was chosen for the MLPs, and the cutoff was set to 6 Å. The number of neurons in each hidden layer of the embedding net and the fitting net was [25, 50, 100] and [240, 240, 240], respectively. The MLPs were trained in 2×10^5 steps, with each step using a batch size of 1. During learning, the learning rate was reduced exponentially from 5×10^{-3} to 1×10^{-8}, where the learning rate was updated every 2000 steps. Both energies and atomic forces were included in the loss function for model optimization. The weight for energies in the loss function started from 0.02 and ended at 1, while that for atomic forces started from 1000 and ended at 1. In the first iteration, the training data were Pt(111)/water interfaces extracted from the AIMD trajectory from Ref. 42 (using a snapshot every 50 fs), Pt(111) slab and bulk water.

In the exploration step, new configurations were generated by performing MD simulations based on one of the MLPs trained in the previous step, using the atomic model of the Pt(111)/water interface described in Sec. II A. In each exploration step, MD simulations with various initial configurations were performed at various temperatures. Details on these MD simulations are given in the supplementary material, Sec. S2. Considering that MLPs are expected to be good at interpolating but poor at extrapolating, the deviations in the results predicted by the four MLPs trained in the previous step can be used to estimate in how far a given configuration is already represented by the existing training dataset. Configurations for which the deviations in atomic forces lay between 0.12 and 0.25 eV/Å were selected as candidates to form additional training data. In each iteration, a certain number of these candidate configurations (150 for the first 16 iterations and 100 for the remaining iterations) was chosen randomly from the candidate structures and added to the training dataset.

In the labeling step, DFT calculations were performed for the selected configurations from the exploration step with the computational setup specified above.

After 24 iterations of the concurrent learning workflow, the MLP trained on the collected dataset showed good accuracy and generalizability. A final training with 2×10^6 training steps (instead of 2×10^5 as used during training) was performed. Note that the initial training dataset obtained from AIMD trajectories was discarded after the first few training iterations. The MLP obtained in the final training step shows root mean square errors (RMSEs) of 0.43 meV/atom and 58.73 meV/Å for energies and atomic forces, respectively. Moreover, some important thermodynamic and dynamic properties of interfacial water were described well as detailed in the supplementary material, Sec. S1.

C. Electronic dielectric constant calculation

While the MLP used in this work enables the simulation up to nanoseconds, only energies and atomic forces can be predicted. To compute the electronic dielectric constant, we perform DFT calculations for several snapshots from the molecular dynamics trajectory to determine the density response to a small, perturbing electric field.[23] By averaging over the density response (or equivalently the inverse dielectric constant) for several snapshots, a converged dielectric profile can be obtained, as described below.

Without loss of generality, we will formulate the calculation in the z direction, which is the direction parallel to the surface normal in our case.

We start by defining an "external" electric field $\mathscr{E}_{\mathrm{vac}}$, which corresponds to the electric field in a vacuum region outside the system,

$$\mathscr{E}_{\mathrm{vac}} = \left.\frac{\mathrm{d}V}{\mathrm{d}z}\right|_{z=z_{\mathrm{vac}}}, \tag{1}$$

where V is the Hartree potential averaged over x and y and z_{vac} is a position in the vacuum region [see Fig. 1(b)]. The field $\mathscr{E}_{\mathrm{vac}}$ is related to the electric displacement $\mathscr{D}$ via $\mathscr{D} = \varepsilon_0 \mathscr{E}_{\mathrm{vac}}$, where ε_0 is the vacuum permittivity. To determine the electronic dielectric contribution, we analyze the effect of applying such an external field to several snapshots taken from the molecular dynamics trajectory while keeping the nuclei fixed. A small change from $\mathscr{E}_{\mathrm{vac}}$ to $\mathscr{E}_{\mathrm{vac}} + \Delta\mathscr{E}_{\mathrm{vac}}$ gives rise to a change in charge density,

$$\Delta\rho(z;\mathscr{E}_{\mathrm{vac}}) = \rho(z;\mathscr{E}_{\mathrm{vac}} + \Delta\mathscr{E}_{\mathrm{vac}}) - \rho(z;\mathscr{E}_{\mathrm{vac}}), \tag{2}$$

where $\rho(z,\mathscr{E}_{\mathrm{vac}})$ is the (electronic) charge density averaged over x and y, at height z and an external field $\mathscr{E}_{\mathrm{vac}}$. From the charge density difference $\Delta\rho$, the change in polarization ΔP can be calculated via

$$\nabla \cdot \Delta P(z;\mathscr{E}_{\mathrm{vac}}) = -\Delta\rho(z;\mathscr{E}_{\mathrm{vac}}). \tag{3}$$

The polarization P affects the electric field $\mathscr{E}$ felt within the system, as $\mathscr{E} = \mathscr{E}_{\mathrm{vac}} - \varepsilon_0^{-1} P$. Therefore, when the external field is changed by $\Delta\mathscr{E}_{\mathrm{vac}}$, the change in the electric field at position z will be given by

$$\Delta\mathscr{E}(z;\mathscr{E}_{\mathrm{vac}}) = \Delta\mathscr{E}_{\mathrm{vac}} - \varepsilon_0^{-1}\Delta P(z;\mathscr{E}_{\mathrm{vac}}). \tag{4}$$

Combining Eqs. (3) and (4), and using the definition of the dielectric constant $\mathscr{E}_{\mathrm{vac}} = \varepsilon_r \mathscr{E}$, the inverse, z-resolved electronic dielectric constant $1/\varepsilon_{\mathrm{elec}}$ at the given external electric field $\mathscr{E}_{\mathrm{vac}}$ can be determined from

$$\varepsilon_{\mathrm{elec}}^{-1}(z;\mathscr{E}_{\mathrm{vac}}) = \frac{\Delta\mathscr{E}(z;\mathscr{E}_{\mathrm{vac}})}{\Delta\mathscr{E}_{\mathrm{vac}}} = \frac{\Delta\mathscr{E}_{\mathrm{vac}} - \varepsilon_0^{-1}\Delta P(z;\mathscr{E}_{\mathrm{vac}})}{\Delta\mathscr{E}_{\mathrm{vac}}}. \tag{5}$$

The inverse electronic dielectric constant obtained in this way can then be averaged over several snapshots from the molecular dynamics trajectory to obtain a converged dielectric profile. (Note that this is the electronic dielectric response only, as the nuclei are frozen in this approach.)

For this approach to work, we still require well-defined boundary conditions for Eq. (3). These can be obtained either by using an approach based on Wannier centers and the Berry-phase polarization as sketched in Ref. 23, or by introducing a vacuum layer and setting P to zero in a region where $\rho = 0$ (i.e., in the vacuum region). Introducing a vacuum layer in the center of the Pt slab is no option, as the applied field would then be completely shielded in the water region by the two metal electrodes. Therefore, half-cell configurations with only one metal–water interface are extracted from various snapshots of the MD trajectory as follows: All Pt atoms and all water molecules residing at $z \leq 13$ Å from the Pt surface are kept, and a vacuum layer of 30 Å is inserted, leading to cells as shown in Fig. 1(b). Based on the test shown in the supplementary material, Sec. S3, a water thickness of 13 Å is sufficient to eliminate the influence of the water–vacuum interface on the water–metal interface up to a few Angstrom away from the surface. In the resulting half-cell configurations, an external field $\mathscr{E}_{\text{vac}}$ (or $\mathscr{E}_{\text{vac}} + \Delta\mathscr{E}$) can be applied indirectly in CP2K by using the implicit (generalized) Poisson solver and specifying Dirichlet boundary conditions (DBCs).[47]

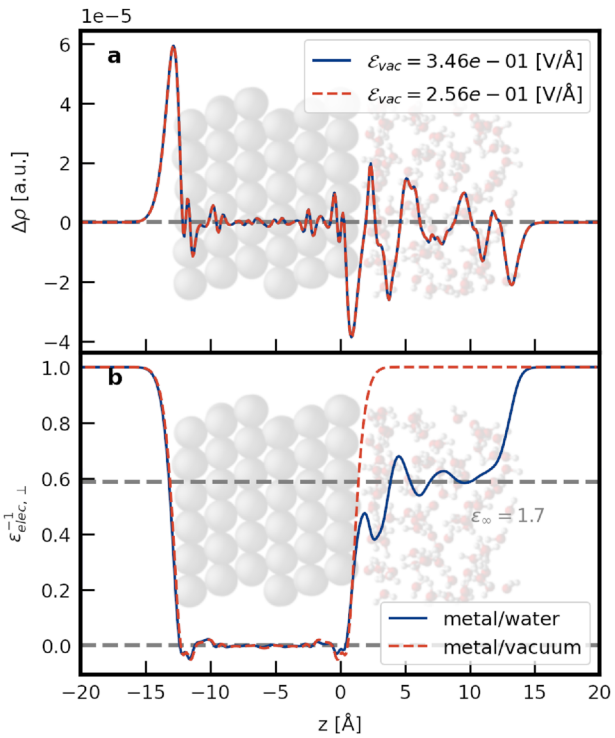

FIG. 2. (a) Charge density difference $\Delta\rho$ for a single snapshot obtained when changing the external field from $\mathscr{E}_{\text{vac}}$ to $\mathscr{E}_{\text{vac}} + \Delta\mathscr{E}_{\text{vac}}$, where the perturbing external field $\Delta\mathscr{E}_{\text{vac}}$ is 0.09 V/Å. The strong independence of polarization charges $\Delta\rho$ on the value of $\mathscr{E}_{\text{vac}}$ suggests a linear response behavior. The blue solid and red dashed lines, denoting different values of $\mathscr{E}_{\text{vac}}$ applied, overlap. (b) Inverse electronic dielectric profile obtained from the polarization charges and averaging over several snapshots. z coordinates are given relative to the average position of the outermost Pt atoms at the metal–water interface.

Since we are interested in the electronic dielectric constant under conditions of zero charge, it may seem appropriate to set $\mathscr{E}_{\text{vac}}$ to zero. However, we deviate from this choice to account for the specific computational setup used here and to avoid unphysical band misalignment issues. The way in which this is done is explained and rationalized in detail in Sec. S4 of the supplementary material. Since it is possible to obtain a linear behavior in $\mathscr{E}_{\text{vac}}$ once the band alignment issues are accounted for [see Fig. 2(a) and Fig. S13 of the supplementary material], we believe the deviation from $\mathscr{E}_{\text{vac}} = 0$ to be of little physical significance and the extracted electronic dielectric constant to represent the electronic dielectric constant at the pzc well.

III. RESULTS

A. Electronic dielectric response at the Pt(111)/water interface

To obtain the electronic polarizability of the Pt(111)/water interface, we proceed as detailed in Sec. II C. The polarization charge profile obtained for a representative snapshot is shown in Fig. 2(a). As expected, large polarization charges are observed at the metal/vacuum interface. These polarization charges shield the electric field inside the metal. The shielding does not occur at the center of the outermost Pt atoms but slightly beyond the edge, as expected due to the electron spillover at metal surfaces.[48,49] At the metal/water interface, the shielding is partially lifted, as evidenced by a negative peak with an integrated total charge slightly smaller than that at the metal/vacuum interface. In the water region, the polarization charges fluctuate. These fluctuations reflect the layering of the water molecules and electronic polarization occurring within each layer. A negative peak in the polarization charges at the water/vacuum interface indicates that the polarization is lifted there.

The inverse electronic dielectric profile can be obtained from the polarization charges via Eq. (5). By averaging over 34 snapshots separated by 100 ps, a converged profile is obtained as shown in Fig. 2(b). Convergence tests can be found in Sec. S5 of the supplementary material. As expected, the inverse of the electronic dielectric constant is close to zero within the metal slab, indicating nearly perfect conductivity. Interestingly, a negative inverse dielectric constant is observed at the metal edges. Such a negative dielectric response has been observed earlier and can be rationalized as an indication of Le Châtelier's principle: Positive polarization charges increase the electrostatic potential within metal with respect to vacuum. At the same time, the electron spillover will decrease, effectively moving the image charge plane inward as the surface charge increases (and outward as the surface charge becomes increasingly negative). This effect is captured in a negative polarizability in the region in which the image charge plane shifts.[50]

In the water region, the electronic dielectric constant rapidly decays to a value close to the experimental optical dielectric constant of water $\varepsilon_r^\infty \approx 1.7$.[30] This is expected as we consider only the electronic response here (the nuclei are fixed in each snapshot and cannot contribute to the dielectric constant as extracted from applying an external field).

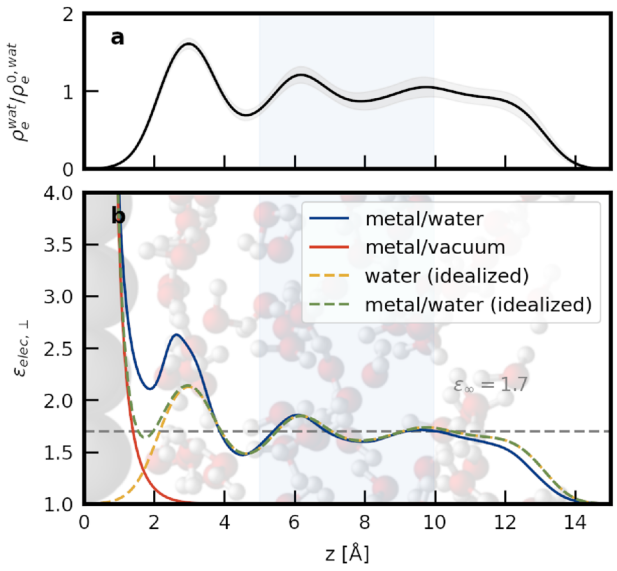

FIG. 3. (a) Atom density-derived electron density profile of water relative to the "bulk" value $\rho_e^{e,wat}$ as approximated by the density between 5 and 10 Å (blue shaded region). (b) Electronic dielectric profile as obtained from the polarization charges and averaging over several snapshots for the metal/water (blue line) and metal/vacuum (red line) interfaces. Yellow line: dielectric profile expected for the structured water at the interface only [Eq. (6)]. Green line: idealized dielectric profile expected for a "non-interacting" metal/water interface [Eq. (7)]. The z-coordinates are relative to the average positions of the outermost Pt atoms at the metal–water interfaces.

In the interfacial region, the behavior of the electronic dielectric constant is more complex. When approaching the interface from the bulk water side, for $z \lesssim 7$ Å, the dielectric response oscillates. A visual comparison with the snapshot of the atomic structure underlain in Fig. 3(b) shows that these oscillations correlate with the water density. To quantify this effect, we approximate the valence electron density $\rho_e^{wat}(z)$ of the water by placing Gaussian distributions with an amplitude equal to the valence electron number and a width equal to the atomic radii on each atom in the water region and average over all snapshots. This results in the approximate valence electron density shown in Fig. 3(a). Using this electron density, we can compute an idealized, density-scaled water dielectric response as

$$\varepsilon_{elec}^{id.\,water}(z) = 1 + \chi^{wat}\frac{\rho_e^{wat}(z)}{\rho_e^{0,wat}}, \tag{6}$$

where $\chi^{wat} = 1.7 - 1$ is the electronic dielectric susceptibility of water and $\rho_e^{0,wat}$ is the valence electron density in bulk water region indicated by the blue shade in Fig. 3.

As shown in Fig. 3(b), the density-scaled water electronic dielectric constant (yellow dashed line) captures the dielectric constant (blue solid line) well for $z \gtrsim 3.7$ Å. This suggests that the electronic dielectric response in this region is still dominated by the "pure" water response and is only modulated by the water structuring near the interface. As we move closer to the interface, we expect the dielectric response of the metal to play a role as well.

To account for the metal at the interface in an idealized fashion, we now add the dielectric susceptibility that one would obtain at the metal/vacuum interface ($\chi^{metal/vac}(z) = 1 - \varepsilon_{elec}^{metal/vac}$) to the density-scaled water response from Eq. (6) to obtain an idealized electronic dielectric response of the interface,

$$\varepsilon_{elec}^{id.\,metal/water}(z) = 1 + \chi^{metal/vac}(z) + \chi^{wat}\frac{\rho_e^{wat}(z)}{\rho_e^{0,wat}}. \tag{7}$$

This idealized response can explain the actual response of the metal/water interface for $z \lesssim 1$ Å and $z \gtrsim 3.7$ Å. In between, the actual dielectric response deviates from our idealized model. This interstitial region coincides with the region in which a pronounced electron redistribution due to metal/water interactions is expected.[42]

To visualize the effect of electron redistribution at the metal/water interface, we show in Fig. 4 the molecular orbitals calculated for water monomers in contact with Pt(111) slabs in typical "H-down" (physisorbed) and "O-down" (chemisorbed) configurations.[51] Compared to their gas phase counterparts, the water molecules in contact with metal clearly show elongated molecular orbitals. This will not only enhance the electron density in the interfacial region, but the more diffuse orbitals can also be expected to enhance the polarizability of the molecule.[52]

In an effort to quantify the enhanced polarizability, we compute the changes in the location of the maximally localized Wannier

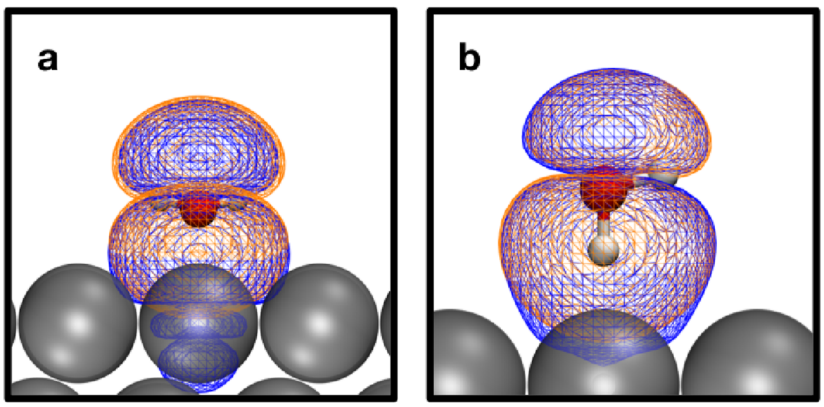

FIG. 4. Valence orbital of a "chemisorbed" (H-up) (a) and a "physisorbed" (H-down) (b) water molecule near the surface (blue) compared with the orbital that one would find for a molecule in the same geometry in gas phase (orange). The isosurfaces are illustrated with an isovalue of 0.01 e/bohr.[3]

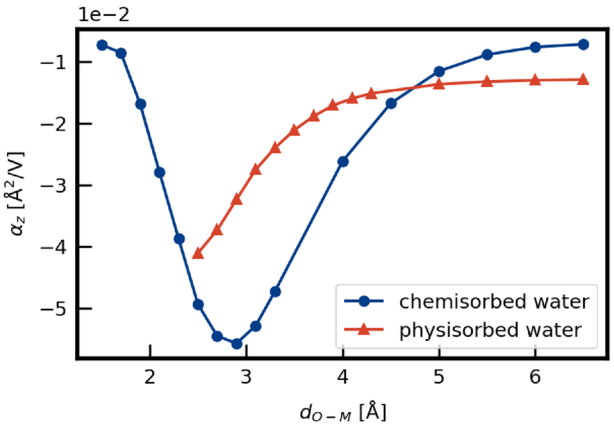

FIG. 5. Orbital polarizability as defined in Eq. (8) for single water molecules above the surface as a function of metal–water distances. "Chemisorbed" refers to water molecules in H-up geometry, and "physisorbed" refers to water molecules in H-down geometries. In both cases, the oxygen atoms are located at the top sites of metal slab.

centers (MLWCs) when applying a small electric field (see Sec. S6 of the supplementary material for computational details). Considering that the electronic polarization of a molecule is a consequence of shifts in charge centers due to an applied electric field, the changes in the location of MLWCs caused by a change in electric field should allow quantifying the "polarizability of an orbital" in the z-direction by

$$\alpha_z = \frac{\Delta z_w}{\Delta \mathscr{E}_{\text{vac}}}, \tag{8}$$

where Δz_w is the shift in the MLWCs induced by a change in the electric field in vacuum $\Delta\mathscr{E}_{\text{vac}}$. In Fig. 5, we show how the z-resolved orbital polarizability of the orbital pointing maximally to the metal varies with the metal–water distances. Clearly, the polarizability α_z of these metal–water "bonding" orbitals increases drastically for water molecules residing close to the metal surface. The enhanced polarizability at the interface compared to the simplified model from Eq. (7) can thus be expected not to be caused purely by an increase in the electronic density, but rather by a more flexible electron cloud in the bonding region.

Overall, the electronic response at the interface can thus be considered to be well described by the summation of effects from the idealized metal and idealized water, with deviations due to more diffuse and polarizable orbitals in the contact region between metal and water (i.e., 1 Å $\lesssim z \lesssim$ 3.7 Å). The influence of more polarizable orbitals is relatively small though, enhancing the dielectric constant only by about 25%. Importantly, the electronic dielectric response $\varepsilon_{\text{elec}}$ at the interface remains lower than $\varepsilon_{\text{elec}} < 2.8$ (i.e., only one point higher than in bulk solution) as soon as the response of the bare metal response has decayed for $z \gtrsim 1$ Å. This is interesting insofar as we do not expect the orientational and ionic dielectric response to contribute to the overall dielectric constant for z-values below 1.5 Å (see supporting information, Sec. S7, for more details). This suggests the presence of a "gap" region between the metal and the water in which the total dielectric constant is low (much lower than the average dielectric constant expected in the Helmholtz layer of 6), confining the majority of the potential drop to this region. To underline this statement, we also compute the orientational dielectric constant. As discussed in Sec. S6 of the supplementary material and shown in Fig. S14, the orientational dielectric response can indeed be expected to kick in only for $z \gtrsim 1.5$ Å from the surface, leaving a "gap" region between $z \approx 1$ Å and $z \approx 1.5$ Å in which the dielectric constant should not be much larger than 2.8. Note that we refrain from trying to add the orientational and electronic contributions. Adding dielectric constants (or polarizabilities, to be more exact) is not straightforward if the polarizabilities are not constant in space, as shown in Ref. 53. The authors are not aware of any method that would allow adding contributions if one of them (the electronic part in our case) contains regions with metallic behavior. The argument given above about the orientational dielectric response only kicking in at larger distances should, therefore, be seen as a qualitative statement.

IV. DISCUSSION

A. From dielectric profile to double layer capacitance

Building on the idea that the dielectric response will be dominated by the electronic dielectric response for distances up to ~1.5 Å from the surface, we can investigate the influence of the relatively weak electronic dielectric response between the image charge plane and the first water layer on the double layer capacitance. To this end, we approximate the interfacial capacitance as two capacitors in series: capacitor C_1, which extends from the metal to approximately $z_s = 1.5$ Å from the surface (a region in which the dielectric response should be dominated by the electronic contribution), and capacitor C_2, in which we expect the ionic and orientational dielectric response of the water to start playing a role. This situation is sketched in Fig. 6. Assuming that only the electronic dielectric response is relevant for C_1, we can compute its value as

$$C_1 = \varepsilon_0^{-1} \int_{z_m}^{z_s} \frac{1}{\varepsilon_{\text{elec}}}\, \mathrm{d}z = \varepsilon_0^{-1} \overline{\varepsilon_{\text{elec}}^{-1}} \Delta z, \tag{9}$$

where the lower integration bound z_m should be located somewhere in the metal electrode, $\Delta z = z_s - z_m$, and $\overline{\varepsilon_{\text{elec}}^{-1}}$ is the average inverse electronic dielectric response in the region $z \in [z_m, z_s]$. Note that the exact choice of z_m only impacts $\overline{\varepsilon_{\text{elec}}^{-1}}$ but not the value of C_1 as long as $\varepsilon_{\text{elec}}^{-1} \approx 0$ in the metal. Moreover, the capacitive contribution from the electron spillover at metal surfaces can be considered in this way. This leads to a z_s-dependent value of C_1 as sketched in Fig. 6. Adding capacitor C_2 in series will decrease the overall interfacial capacitance, C, compared to C_1 (unless C_2 is negative). Since C_1 is limited to 40 μF/cm^2 at $z_s = 1.5$ Å, this suggests that the overall interfacial capacitance $C = (C_1^{-1} + C_2^{-1})^{-1}$ on Pt(111) should also be limited to values lower than 40 μF/cm^2, as shown in Fig. 6. This is in good agreement with capacitance values found experimentally far away from the potential of zero charge at several metal/water interfaces: These capacitances typically take values around 20 μF/cm^2. However, in concentrated electrolytes, close to the potential of zero charge, large capacitance values of 65 to 100 μF cm^2 have been found experimentally for several single crystalline surfaces, including Pt(111),[29] Au(111),[54] Ag(110)[55], and Ag(100).[56] Such high capacitance values cannot be explained by the dielectric response of water (not even when assuming ε_r to

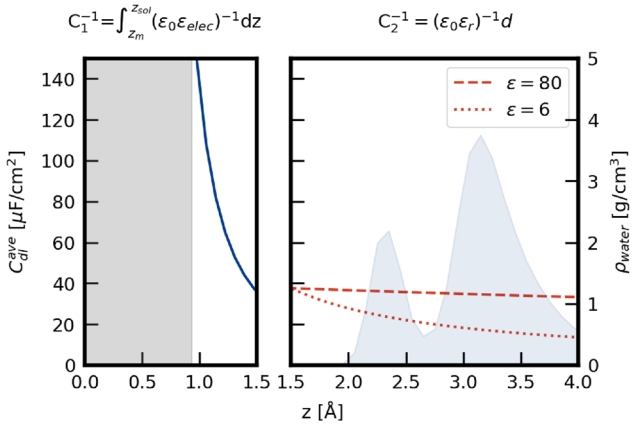

FIG. 6. Average capacitance C_{dl}^{ave} up to a certain distance z from the metal surface. Up to $z = 1.5$ Å (blue line), for $C_1(z)$, only the electronic response is taken into account. For C_2, a larger dielectric constant is considered to account for the electronic, orientational, and ionic response. Red dashed line: $C(z) = \left[C_1(1.5\,\text{Å})^{-1} + C_2(d = z - 1.5\,\text{Å})^{-1}\right]^{-1}$ using $\varepsilon_r = 80$ in C_2; red dotted line: $C(z) = \left[C_1(1.5\,\text{Å})^{-1} + C_2(d = z - 1.5\,\text{Å})^{-1}\right]^{-1}$ using $\varepsilon_r = 6$. The gray shade indicates the region between the metal surface and the image charge plane. The blue shade indicates the water density distribution in the z-direction.

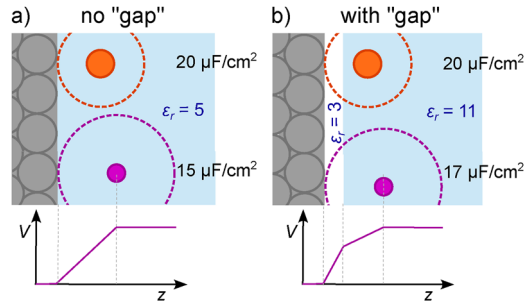

FIG. 7. Sketch of two interfaces, one with a constant ε_r (a) and the other with a region of low dielectric constant close to the interface and a higher ε_r thereafter (b). Lower panels: sketch of the resulting potential profile.

be 80 in the water region), suggesting that these peaks can also not be a (pure) consequence of dielectric saturation, i.e., all water dipoles being already aligned reducing ε_r as the surface electric field increases, as often assumed.[27,29,57,58] Instead, other effects such as pseudo-capacitances or water ad-/desorption[59] must play a role.

B. From dielectric response to electrocatalysis

To further emphasize the potential relevance of a region with a low dielectric response on electrocatalysis, we discuss two case studies: (i) the expected change in surface electric field with changing cation size and (ii) the influence of the potential profile on electrochemical kinetics. Care should be taken not to over-interpret the qualitative discussions as, likely, the presence of reactants at the interface will influence the dielectric profile and as a reaction may "feel" a local, non-time averaged dielectric response rather than the time-averaged response.[60] Nevertheless, the qualitative picture sketched in the following should hold.

1. Ion size effect on the surface electric field

The surface electric field can play a crucial role in electrochemical reactions, as it can stabilize dipolar (adsorbed) species, such as adsorbed $^*CO_2$—a crucial intermediate in CO_2 reduction.[61] Ringe *et al.* invoked this idea for example to explain the dependence of the CO_2 reduction rate on the ionic species in the electrolyte.[3] The idea behind this ion size effect is that different ions approach the surface more or less closely, leading to differences in the double-layer capacitance and, hence, differences in the surface electric field at a given potential. The extent to which different ion sizes affect the double-layer capacitance, however, depends sensitively on the dielectric profile of the interface as illustrated in Fig. 7. When ε_r is constant at $\varepsilon_r = 5$, a change in (hydrated) ion radius (or ion position relative to the image charge plane) from $r = 2.3$ to $r = 3$ would change the capacitance by 27% from 20 to 15 μF cm^2. Meanwhile, if ε_r changes from $\varepsilon_r = 3$ for $z \in [1,2]$ Å to $\varepsilon_r = 11$ thereafter, the same change in ion position would only cause a 13% decrease in the capacitance. As the surface electric field at constant potential is proportional to the capacitance, this suggests a much smaller (relative) change in the surface electric field in the latter case. Considering the low polarizability that we find in the region of 1 Å to ≥ 1.5 Å, one may thus expect the ion size to have a smaller effect on the interfacial electric field than naively expected.

2. Potential profile and electrochemical reaction kinetics

Electrochemical reaction kinetics can be expected to depend on the potential profile. This is captured, for example, in the Frumkin correction to the Butler–Volmer equation.[11,12] Similarly, one may expect transition state energies of charge transfer reactions to depend on the potential present at the position of the center of charge of the transition state. This potential will, however, depend on the dielectric profile, as depicted in Fig. 7. When the double layer is marked by a "gap" region close to the interface, the potential increases rapidly to the applied potentials when moving away from the interface. For a constant ε_r, the potential continues to increase considerably over a much wider range of distances from the surface, leading to a different Frumkin correction.

Taken together, this showcases the immediate relevance of a region with a small dielectric constant above a Pt surface, as found in this work.

V. SUMMARY AND CONCLUSIONS

In summary, we have computed the electronic dielectric response at the Pt(111)/water interface. We find the interfacial dielectric response to be reasonably well captured by a combination of the response of the metal at a metal/vacuum interface and the electronic response of bulk water scaled by the surface-near (valence charge) density of the water. Deviations can be explained by the molecular orbitals of water molecules in contact with the Pt surface being more diffuse, leading to a somewhat increased polarizability of these orbitals. In spite of the resulting enhancement of the dielectric response at the interface, the electronic dielectric constant remains below 2.8 once the electronic response of the metal has decayed at

~1 Å from the center of the outermost Pt layer. Since the first water molecules do not approach the surface any more closely than 2.0 Å, the low electronic dielectric constant at the interface suggests the presence of a "gap" region between the image charge plane of the metal and the first water layer in which the dielectric constant should be small. This conclusion has important implications on the double layer capacitance and the potential profile at the surface, which in turn can influence electrochemical reactions.

SUPPLEMENTARY MATERIAL

The following information can be found in the supplementary material: (1) validation of the machine-learned potential (energies and atomic forces, water structure, and water dynamics); (2) setup of MD sampling in the concurrent learning workflow; (3) water thickness convergence test; (4) details on the extraction of the electronic and orientational dielectric constant; (5) convergence tests of the electronic dielectric constant; (6) computational setup for maximal localized Wannier center calculation; and (7) orientational dielectric constant at the interface.

ACKNOWLEDGMENTS

J.-X.Z. acknowledges the Xiamen University and iChEM for a Ph.D. studentship and financial support by the Graduate School of Xiamen University for an internship at Leiden University. J.C. acknowledges funding from the National Science Fund for Distinguished Young Scholars (Grant No. 22225302), the National Natural Science Foundation of China (Grant Nos. 92161113, 21991151, 21991150, and 22021001), the Fundamental Research Funds for the Central Universities (Grant Nos. 20720220008, 20720220009, and 20720220010), Laboratory of AI for Electrochemistry (AI4EC), and IKKEM (Grant Nos. RD2023100101 and RD2022070501). The authors thank Harry Stern for discussions.

AUTHOR DECLARATIONS

Conflict of Interest

The authors have no conflicts to disclose.

Author Contributions

Jia-Xin Zhu: Conceptualization (supporting); Data curation (lead); Formal analysis (lead); Funding acquisition (supporting); Investigation (lead); Methodology (equal); Software (lead); Validation (lead); Visualization (equal); Writing – original draft (equal); Writing – review & editing (equal). **Jun Cheng**: Conceptualization (supporting); Funding acquisition (lead); Methodology (supporting); Resources (lead); Supervision (supporting); Writing – review & editing (supporting). **Katharina Doblhoff-Dier**: Conceptualization (lead); Data curation (supporting); Formal analysis (supporting); Investigation (supporting); Methodology (equal); Project administration (lead); Resources (lead); Supervision (lead); Validation (supporting); Visualization (equal); Writing – original draft (equal); Writing – review & editing (equal).

DATA AVAILABILITY

The data that support the findings of this study are available in Zenodo repository at https://doi.org/10.5281/zenodo.13761448.

REFERENCES

[1] A. J. Bard and L. R. Faulkner, *Electrochemical Methods: Fundamentals and Applications* (Wiley, 2000), Vol. 50.
[2] W. Schmickler and E. Santos, *Interfacial Electrochemistry* (Springer, Berlin, Heidelberg, 2010).
[3] S. Ringe, E. L. Clark, J. Resasco, A. Walton, B. Seger, A. T. Bell, and K. Chan, "Understanding cation effects in electrochemical CO_2 reduction," Energy Environ. Sci. **12**, 3001–3014 (2019).
[4] M. C. O. Monteiro, F. Dattila, B. Hagedoorn, R. García-Muelas, N. López, and M. T. M. Koper, "Absence of CO_2 electroreduction on copper, gold and silver electrodes without metal cations in solution," Nat. Catal. **4**, 654–662 (2021).
[5] M. C. O. Monteiro, F. Dattila, N. López, and M. T. M. Koper, "The role of cation acidity on the competition between hydrogen evolution and CO_2 reduction on gold electrodes," J. Am. Chem. Soc. **144**, 1589–1602 (2021).
[6] Y.-S. Hsu, S. T. Rathnayake, and M. M. Waegele, "Cation effects in hydrogen evolution and CO_2-to-CO conversion: A critical perspective," J. Chem. Phys. **160**, 160901 (2024).
[7] M. C. O. Monteiro, A. Goyal, P. Moerland, and M. T. M. Koper, "Understanding cation trends for hydrogen evolution on platinum and gold electrodes in alkaline media," ACS Catal. **11**, 14328–14335 (2021).
[8] A. Goyal and M. T. M. Koper, "The interrelated effect of cations and electrolyte pH on the hydrogen evolution reaction on gold electrodes in alkaline media," Angew. Chem., Int. Ed. **60**, 13452–13462 (2021).
[9] A. H. Shah, Z. Zhang, Z. Huang, S. Wang, G. Zhong, C. Wan, A. N. Alexandrova, Y. Huang, and X. Duan, "The role of alkali metal cations and platinum-surface hydroxyl in the alkaline hydrogen evolution reaction," Nat. Catal. **5**, 923–933 (2022).
[10] J. T. Bender, A. S. Petersen, F. C. Østergaard, M. A. Wood, S. M. J. Heffernan, D. J. Milliron, J. Rossmeisl, and J. Resasco, "Understanding cation effects on the hydrogen evolution reaction," ACS Energy Lett. **8**, 657–665 (2022).
[11] A. Frumkin, "Wasserstoffüberspannung und Struktur der Doppelschicht," Z. Phys. Chem. **164A**, 121–133 (1933).
[12] A. N. Frumkin, "Influence of cation adsorption on the kinetics of electrode processes," Trans. Faraday Soc. **55**, 156 (1959).
[13] G. Kastlunger, P. Lindgren, and A. A. Peterson, "Controlled-potential simulation of elementary electrochemical reactions: Proton discharge on metal surfaces," J. Phys. Chem. C **122**, 12771–12781 (2018).
[14] N. G. Hörmann, O. Andreussi, and N. Marzari, "Grand canonical simulations of electrochemical interfaces in implicit solvation models," J. Chem. Phys. **150**, 041730 (2019).
[15] M. M. Melander, M. J. Kuisma, T. E. K. Christensen, and K. Honkala, "Grand-canonical approach to density functional theory of electrocatalytic systems: Thermodynamics of solid–liquid interfaces at constant ion and electrode potentials," J. Chem. Phys. **150**, 041706 (2018).
[16] M. M. Melander, T. Wu, T. Weckman, and K. Honkala, "Constant inner potential DFT for modelling electrochemical systems under constant potential and bias," npj Comput. Mater. **10**, 5 (2024).
[17] R. Sundararaman, K. Letchworth-Weaver, and K. A. Schwarz, "Improving accuracy of electrochemical capacitance and solvation energetics in first-principles calculations," J. Chem. Phys. **148**, 144105 (2018).
[18] S. Ringe, N. G. Hörmann, H. Oberhofer, and K. Reuter, "Implicit solvation methods for catalysis at electrified interfaces," Chem. Rev. **122**, 10777–10820 (2021).
[19] R. Sundararaman, K. A. Schwarz, K. Letchworth-Weaver, and T. A. Arias, "Spicing up continuum solvation models with SaLSA: The spherically averaged liquid susceptibility *ansatz*," J. Chem. Phys. **142**, 054102 (2015).
[20] R. Sundararaman and W. A. Goddard, "The charge-asymmetric nonlocally determined local-electric (CANDLE) solvation model," J. Chem. Phys. **142**, 064107 (2015).

[21] F. Nattino, M. Truscott, N. Marzari, and O. Andreussi, "Continuum models of the electrochemical diffuse layer in electronic-structure calculations," J. Chem. Phys. **150**, 041722 (2018).
[22] O. Andreussi, N. G. Hörmann, F. Nattino, G. Fisicaro, S. Goedecker, and N. Marzari, "Solvent-aware interfaces in continuum solvation," J. Chem. Theory Comput. **15**, 1996–2009 (2019).
[23] F. Giustino and A. Pasquarello, "Theory of atomic-scale dielectric permittivity at insulator interfaces," Phys. Rev. B **71**, 144104 (2005).
[24] B. E. Conway, J. O. Bockris, and I. A. Ammar, "The dielectric constant of the solution in the diffuse and Helmholtz double layers at a charged interface in aqueous solution," Trans. Faraday Soc. **47**, 756 (1951).
[25] R. Parsons, "The structure of the mercury-electrolyte interphase in the presence of thiourea," Proc. R. Soc. London, Ser. A **261**, 79–90 (1961).
[26] M. A. V. Devanathan, "The structure of the electrical double layer in the presence of adsorbed organic molecules," Proc. R. Soc. London, Ser. A **264**, 133–144 (1961).
[27] J. O. Bockris, M. A. V. Devanathan, and K. Müller, "On the structure of charged interfaces," Proc. R. Soc. London, Ser. A **274**, 55–79 (1963).
[28] W. M. Haynes, *CRC Handbook of Chemistry and Physics* (CRC Press, 2014).
[29] T. Pajkossy and D. Kolb, "On the origin of the double layer capacitance maximum of Pt(111) single crystal electrodes," Electrochem. Commun. **5**, 283–285 (2003).
[30] J. Fiedler, M. Boström, C. Persson, I. Brevik, R. Corkery, S. Y. Buhmann, and D. F. Parsons, "Full-spectrum high-resolution modeling of the dielectric function of water," J. Phys. Chem. B **124**, 3103–3113 (2020).
[31] D. J. Bonthuis, S. Gekle, and R. R. Netz, "Dielectric profile of interfacial water and its effect on double-layer capacitance," Phys. Rev. Lett. **107**, 166102 (2011).
[32] D. J. Bonthuis, S. Gekle, and R. R. Netz, "Profile of the static permittivity tensor of water at interfaces: Consequences for capacitance, hydration interaction and ion adsorption," Langmuir **28**, 7679–7694 (2012).
[33] F. Deißenbeck, C. Freysoldt, M. Todorova, J. Neugebauer, and S. Wippermann, "Dielectric properties of nanoconfined water: A canonical thermopotentiostat approach," Phys. Rev. Lett. **126**, 136803 (2021).
[34] B. Tran, Y. Zhou, M. J. Janik, and S. T. Milner, "Negative dielectric constant of water at a metal interface," Phys. Rev. Lett. **131**, 248001 (2023).
[35] H. Heinz, R. A. Vaia, B. L. Farmer, and R. R. Naik, "Accurate simulation of surfaces and interfaces of face-centered cubic metals using 12–6 and 9–6 Lennard-Jones potentials," J. Phys. Chem. C **112**, 17281–17290 (2008).
[36] L. Scalfi, M. Salanne, and B. Rotenberg, "Molecular simulation of electrode-solution interfaces," Annu. Rev. Phys. Chem. **72**, 189–212 (2021).
[37] F. Deißenbeck and S. Wippermann, "Dielectric properties of nanoconfined water from *ab initio* thermopotentiostat molecular dynamics," J. Chem. Theory Comput. **19**, 1035–1043 (2023).
[38] X.-Y. Li, X.-F. Jin, X.-H. Yang, X. Wang, J.-B. Le, and J. Cheng, "Molecular understanding of the Helmholtz capacitance difference between Cu(100) and graphene electrodes," J. Chem. Phys. **158**, 084701 (2023).
[39] Y. Ando, Y. Gohda, and S. Tsuneyuki, "*Ab initio* molecular dynamics study of the Helmholtz layer formed on solid–liquid interfaces and its capacitance," Chem. Phys. Lett. **556**, 9–12 (2013).
[40] T. D. Kühne, M. Iannuzzi, M. Del Ben, V. V. Rybkin, P. Seewald, F. Stein, T. Laino, R. Z. Khaliullin, O. Schütt, F. Schiffmann, D. Golze, J. Wilhelm, S. Chulkov, M. H. Bani-Hashemian, V. Weber, U. Borštnik, M. Taillefumier, A. S. Jakobovits, A. Lazzaro, H. Pabst, T. Müller, R. Schade, M. Guidon, S. Andermatt, N. Holmberg, G. K. Schenter, A. Hehn, A. Bussy, F. Belleflamme, G. Tabacchi, A. Glöß, M. Lass, I. Bethune, C. J. Mundy, C. Plessl, M. Watkins, J. VandeVondele, M. Krack, and J. Hutter, "CP2K: An electronic structure and molecular dynamics software package-Quickstep: Efficient and accurate electronic structure calculations," J. Chem. Phys. **152**, 194103 (2020).
[41] J. Zeng, D. Zhang, D. Lu, P. Mo, Z. Li, Y. Chen, M. Rynik, L. Huang, Z. Li, S. Shi, Y. Wang, H. Ye, P. Tuo, J. Yang, Y. Ding, Y. Li, D. Tisi, Q. Zeng, H. Bao, Y. Xia, J. Huang, K. Muraoka, Y. Wang, J. Chang, F. Yuan, S. L. Bore, C. Cai, Y. Lin, B. Wang, J. Xu, J.-X. Zhu, C. Luo, Y. Zhang, R. E. A. Goodall, W. Liang, A. K. Singh, S. Yao, J. Zhang, R. Wentzcovitch, J. Han, J. Liu, W. Jia, D. M. York, W. E, R. Car, L. Zhang, and H. Wang, "DeePMD-kit v2: A software package for deep potential models," J. Chem. Phys. **159**, 054801 (2023).
[42] J. Le, M. Iannuzzi, A. Cuesta, and J. Cheng, "Determining potentials of zero charge of metal electrodes versus the standard hydrogen electrode from density-functional-theory-based molecular dynamics," Phys. Rev. Lett. **119**, 016801 (2017).
[43] J. P. Perdew, K. Burke, and M. Ernzerhof, "Generalized gradient approximation made simple," Phys. Rev. Lett. **77**, 3865–3868 (1996).
[44] S. Grimme, J. Antony, S. Ehrlich, and H. Krieg, "A consistent and accurate ab initio parametrization of density functional dispersion correction (DFT-D) for the 94 elements H-Pu," J. Chem. Phys. **132**, 154104 (2010).
[45] Y. Zhang, H. Wang, W. Chen, J. Zeng, L. Zhang, H. Wang, and W. E, "DP-GEN: A concurrent learning platform for the generation of reliable deep learning based potential energy models," Comput. Phys. Commun. **253**, 107206 (2020).
[46] L. Zhang, J. Han, H. Wang, W. A. Saidi, R. Car, and E. Weinan, "End-to-end symmetry preserving inter-atomic potential energy model for finite and extended systems," in *Advances in Neural Information Processing Systems* (Curran Associates Inc., 2018), Vol. 2018, pp. 4436–4446; arXiv:1805.09003.
[47] M. H. Bani-Hashemian, S. Brück, M. Luisier, and J. VandeVondele, "A generalized Poisson solver for first-principles device simulations," J. Chem. Phys. **144**, 044113 (2016).
[48] N. D. Lang and W. Kohn, "Theory of metal surfaces: Work function," Phys. Rev. B **3**, 1215–1223 (1971).
[49] N. D. Lang and W. Kohn, "Theory of metal surfaces: Charge density and surface energy," Phys. Rev. B **1**, 4555–4568 (1970).
[50] W. Schmickler, "Electronic effects in the electric double layer," Chem. Rev. **96**, 3177–3200 (1996).
[51] J. Le, A. Cuesta, and J. Cheng, "The structure of metal–water interface at the potential of zero charge from density functional theory-based molecular dynamics," J. Electroanal. Chem. **819**, 87–94 (2018).
[52] D. Hait and M. Head-Gordon, "When is a bond broken? The polarizability perspective," Angew. Chem., Int. Ed. **62**, e202312078 (2023).
[53] H. A. Stern and S. E. Feller, "Calculation of the dielectric permittivity profile for a nonuniform system: Application to a lipid bilayer simulation," J. Chem. Phys. **118**, 3401–3412 (2003).
[54] T. Pajkossy, T. Wandlowski, and D. M. Kolb, "Impedance aspects of anion adsorption on gold single crystal electrodes," J. Electroanal. Chem. **414**, 209–220 (1996).
[55] G. Valette, "Double layer on silver single-crystal electrodes in contact with electrolytes having anions which present a slight specific adsorption," J. Electroanal. Chem. Interfacial Electrochem. **122**, 285–297 (1981).
[56] G. Valette, "Double layer on silver single crystal electrodes in contact with electrolytes having anions which are slightly specifically adsorbed," J. Electroanal. Chem. Interfacial Electrochem. **269**, 191–203 (1989).
[57] B. Damaskin and A. Frumkin, "Potentials of zero charge, interaction of metals with water and adsorption of organic substances—III. The role of the water dipoles in the structure of the dense part of the electric double layer," Electrochim. Acta **19**, 173–176 (1974).
[58] B. Damaskin, "Model of the dense part of the double layer in the absence of specific adsorption," J. Electroanal. Chem. **75**, 359–370 (1977).
[59] J.-B. Le, Q.-Y. Fan, J.-Q. Li, and J. Cheng, "Molecular origin of negative component of Helmholtz capacitance at electrified Pt(111)/water interface," Sci. Adv. **6**, eabb1219 (2020).
[60] E. Santos and W. Schmickler, "On the timescale of electrochemical processes," Electrochim. Acta **498**, 144659 (2024).
[61] L. D. Chen, M. Urushihara, K. Chan, and J. K. Nørskov, "Electric field effects in electrochemical CO_2 reduction," ACS Catal. **6**, 7133–7139 (2016).